

# Tentative Detection of Electric Dipole Emission from Rapidly Rotating Dust Grains

Douglas P. Finkbeiner<sup>12</sup>, David J. Schlegel

*Princeton University, Department of Astrophysics, Peyton Hall, Princeton, NJ 08544*

and

Curtis Frank

*University of Maryland, Department of Astronomy, College Park, MD 20742-2421*

and

Carl Heiles

*University of California at Berkeley, Department of Astronomy  
601 Campbell Hall, Berkeley, CA 94720*

## ABSTRACT

We present the first tentative detection of spinning dust emission from specific astronomical sources. All other detections in the current literature are statistical. The Green Bank 140 foot telescope was used to observe 10 dust clouds at 5, 8, and 10 GHz. In some cases, the observed emission was consistent with the negative spectral slope expected for free-free emission (thermal bremsstrahlung), but in two cases it was not. One H II region (LPH 201.663+1.643) yields a rising spectrum, inconsistent with free-free or synchrotron emission at the  $\sim 10\sigma$  level. One dark cloud (L 1622) has a similar spectrum with lower significance. Both spectra are consistent with electric dipole emission from rapidly rotating dust grains (“spinning dust”), as predicted by Draine & Lazarian.

*Subject headings:* cosmic microwave background — diffuse radiation — dust, extinction — ISM: clouds — radiation mechanisms: thermal — radio continuum: ISM

---

<sup>1</sup>and University of California at Berkeley, Department of Astronomy

<sup>2</sup>Hubble Fellow

## 1. INTRODUCTION

In the last decade, the *COBE* satellite and several ground- and balloon-based experiments (QMAP, Saskatoon, MAXIMA, BOOMERanG, TOCO, DASI, CBI, and others) have greatly increased our knowledge of the Cosmic Microwave Background (CMB) radiation. Some of these careful observations of the microwave sky have also revealed new and surprising features in the interstellar medium at  $14 < \nu < 53$  GHz. At frequencies above 100 GHz ( $\lambda < 3$  mm), the emission from Galactic cirrus is consistent with thermal emission. This emission is a broken power law, with the break at  $\sim 500$  GHz, interpreted by Finkbeiner *et al.* (1999) as emission from two dust components. Though this interpretation fits the data from 100 to 3000 GHz, a dramatic deviation arises at lower frequencies. This deviation motivates the work presented here.

The *COBE*/DMR data ( $7^\circ$  FWHM) exhibit dust-correlated emission at 90 GHz at approximately the level predicted by a detailed model of the thermal dust spectrum based on DIRBE and FIRAS data (Finkbeiner *et al.* 1999). In the other DMR channels there is a pronounced excess – more than a factor of 10 at 31.5 GHz (Kogut *et al.* 1996). The 19 GHz data from Cottingham’s thesis (Cottingham 1987; Boughn *et al.* 1992) also indicate such an excess (de Oliveira-Costa *et al.* 1998). This microwave excess appears in the Saskatoon experiment as well, but with less significance (de Oliveira-Costa *et al.* 1997). OVRO observations in a ring around the North Celestial Pole at 14 and 31 GHz have demonstrated a correlation of 14 GHz emission with dust at the highest resolution ( $7'$ ) to date, but at a level  $\sim 1000$  times brighter than the expected thermal (vibrational) dust emission (Leitch *et al.* 1997). This excess has been called the “mystery component” (de Oliveira-Costa *et al.* 2001).

The spectral shape of these early measurements is consistent with free-free emission from ionized gas, motivating a comparison with  $H\alpha$  maps. Leitch *et al.* (1997) noted the weakness of  $H\alpha$  emission in the OVRO fields and concluded that only  $T > 10^6$  K gas (e.g. shock-heated gas in a supernova remnant) could produce the observed emission. However, the observed emission would require an energy injection rate at least 2 orders of magnitude greater than that provided by supernovae (Draine & Lazarian 1998a). Another possibility is magnetic dipole emission<sup>3</sup> from ferromagnetic or ferrimagnetic grains, resulting from thermal fluctuations in the magnetization of the grain material. This component is certainly present at some level, but is sub-dominant in the current data (Draine & Lazarian 1999).

The currently favored emission mechanism is electric dipole emission from rapidly rotating dust grains, an idea first proposed by Erickson (1957) and improved upon by Ferrara

---

<sup>3</sup>Note that this mechanism has nothing to do with grain rotation.

& Dettmar (1994). Recent work by Draine & Lazarian (1998b) has refined this idea and shown that ion encounters with dust grains are the dominant spin-up mechanism, leading to concrete predictions of emission as a function of the temperature, density, and ionization fraction of the surrounding gas. This emission mechanism has never been unambiguously observed, but can be made to agree with the observed microwave data for reasonable model parameters. It was previously impossible to tell if the excess emission results from spinning dust or free-free emission, because the predicted spectral slope is similar for  $20 \lesssim \nu \lesssim 40$  GHz, and earlier observations were insufficient to rule out either mechanism. The Tenerife data (de Oliveira-Costa *et al.* 1999) at 10 and 15 GHz have good leverage on the spectral shape, but provide only a statistical detection by cross-correlation. To date, no one has observed spinning dust emission from a specific source.

The spinning dust is expected to have an emission peak at  $\sim 15$  GHz (in temperature units) and be dominated by free-free below  $\sim 5 - 10$  GHz, so by choosing frequencies in this range, one can hope to unambiguously detect this component. We have obtained data for several dust clouds at 5, 8, and 10 GHz, a frequency range over which the spinning dust spectrum differs measurably from that of free-free or synchrotron emission.

## 2. OBSERVING STRATEGY

This study used the NRAO<sup>4</sup> 43m (“140 foot”) telescope at Green Bank shortly before its decommissioning on 1999 July 19. Cassegrain C-band (5 GHz) and X-band (8 – 10 GHz) receivers were used with a 300 MHz bandwidth, and gave a typical system temperature of 30 – 60 K.

Data were obtained during two runs: 22-27 April and 1-6 June, 1999. The nutating subreflector on the 140 foot can switch at up to 2.5 Hz with a 12' throw. Switching is restricted by hardware to a position angle of 292.5° (E of N) for the X-band (8 – 10 GHz) receiver. A second level of switching was accomplished by driving the telescope along the PA = 292.5° direction at a rate of 3' s<sup>-1</sup>, completing a 48' scan every 16 s (Figures 1 and 2). During the scan, the ON-OFF difference was recorded by a digital continuum recorder (DCR) for every chop. The same strip was then observed in the “reverse” direction, a sequence requiring nearly 1 min for a round trip (including turn-around time). During the turn-around time, a calibration noise source was flashed at 1 Hz. In C-band (5 GHz), switching is restricted to a direction orthogonal to the scan line, so switching was not performed at

---

<sup>4</sup>The National Radio Astronomy Observatory is a facility of the National Science Foundation operated under cooperative agreement by Associated Universities, Inc.

5 GHz.

The beam of the 140 foot telescope at 5 GHz (6' FWHM) is well-matched to the SFD98 100 $\mu$ m map, to which the data are compared in §3. At 8 and 10 GHz, multiple parallel scans were performed to subsample a 6' Gaussian beam. For a typical system temperature of 40K and 200ms integration (2Hz switch, so 4 samples per second with 50ms blanking time) we obtain a theoretical sensitivity of 7.3 mK per difference per polarization. Typically 1 hr was spent on each target in each band, yielding a theoretical sensitivity of  $\sim 1$  mK per polarization per pointing. Observations were also attempted at 18 GHz, but the system temperature was too high to obtain any useful data. The 14 GHz receiver was not available at the time of our observing run.

A bandwidth of 300 MHz was used throughout the run. RFI affected a negligible number of the measurements, and these are easily found and discarded later in the analysis.

### 3. ANALYSIS

The Digital Continuum Recorder (DCR) records the difference between the ON position and OFF position some 12' away as the telescope scans over a target. The PA of the chop is fixed at 292.5°, so as not to interfere with point source measurements when scanning E-W or N-S. This arrangement is ideal for point sources, because the OFF never crosses the source and the baseline difference is easily established when the ON position is away from the source. When observing the diffuse ISM, there is no local zero-brightness position to compare to along the scan. We therefore scan parallel to the chop direction to reduce the problem to one dimension.

The measured difference for each chop (Figure 3a) is dominated by sidelobe and atmospheric contamination, and drifts with time. All these effects are generally a smooth function of time, and are removed with a low order polynomial fit with appropriate outlier rejection. The data are then “folded” by plotting as a function of sky position (Figure 3b) to reveal the beam-convolved and differenced structure on the sky. Because of sidelobe and atmospheric contamination, an artificial slope is present in these plots; it is also fit and removed. The data are binned in RA and the median of each bin is overplotted. Note that for the source LPH 201.663+1.643 shown in Figure 3, there is a difference between forward and reverse scans. In the forward direction, the ON position is slightly less than 12' ahead of the OFF position because the telescope is moving east. In the reverse direction, ON is slightly more than 12' away, as the telescope drives west. This means that forward and reverse scans must be analyzed separately, even though they are overplotted in Figure 3b.

Finally, we consider the correlation slope between predicted and observed emission. Because of the double-switched observing strategy, it is impossible to uniquely recover the observed flux of an object. However, a suitable template may be convolved with the same observing strategy and compared to observation. The SFD98 100 $\mu$ m and temperature maps are used to predict a microwave brightness temperature (Figures 3c and 3e) using the factor of 50 $\mu$ K at 10 GHz per  $I_{100\mu\text{m}}$  in MJy/sr (de Oliveira-Costa *et al.* 1999). The correlation slope is then measured and tabulated; it should be consistent with 1 at 10 GHz for a correct prediction, and vary at other frequencies with the shape of the spinning dust spectrum. Separate numbers are tabulated for each combination of polarization and direction (Table 2). The prediction includes a factor of 1/2 for comparison to the single-polarization data. This is why the LCP and RCP measurements are combined by averaging rather than adding them. The (total Stokes I)  $T_B$  per  $I_{100}$  in units of  $\mu\text{K}(\text{ MJy/sr})^{-1}$  may be obtained from Table 2 by multiplying the correlation slopes by 50. Note that L1622 was observed on two occasions at 8.25 GHz.

### 3.1. Calibration

For calibration standards, we use the fits of Salter (2001), who follows Kuehr *et al.* (1981) in using the form  $\log_{10} S = a_0 + a_1 x + a_2 \exp(-x)$  where  $x = \log_{10} \nu$ ,  $\nu$  is in MHz and  $S$  is in Jy. With  $a_0 = 3.523$ ,  $a_1 = -0.779$ , and  $a_2 = -3.732$  for 3C138, we obtain  $S(5, 8.25, 9.75 \text{ GHz}) = (3.54, 2.50, 2.22)$  Jy. This agrees with a simple power-law fit to 87GB (Gregory & Condon 1991) and the Wright *et al.* (1991) survey to within 2%. Cross-checks were done with 3C245 and BL-LAC, and agreed to 5 percent. The definitive calibration was determined by 3C138 however, because it was observed near L1622 and LPH 201.663+1.643 in both space and time.

## 4. RESULTS

Of the targets observed (Table 1) two clouds show significant dust-correlated emission at 5 – 10 GHz. The non-detection of the other targets is not very surprising, because the parameters describing the physical properties of these clouds span a wide range of values, so the relative intensities may vary widely. Both of the detected clouds (Lynds 1622 and LPH 201.663+1.643) show a steep rise from 8 – 10 GHz, with the 5 GHz brightness apparently contaminated by free-free (Table 3). In order to compare these results to previous correlation measurements, results from several experiments are overplotted on the Draine & Lazarian models in Figure 5. All data and model curves are normalized to emission per

H atom for ease of comparison. In practice this is done by normalizing to SFD  $E(B - V)$  values, and then applying a conversion factor. The free-free emission curves corresponding to two values of  $\langle n_e n_p \rangle / \langle n_H \rangle$  are shown, with the upper curve determined by an emission measure derived from the H $\alpha$  survey<sup>5</sup> of Gaustad *et al.* (2001).

Because free-free emission clearly contributes to the measured signal, it is desireable to have an independent limit on the free-free and show that it is consistent with our measurements. This limit may be derived from H $\alpha$  as follows. The emission coefficient  $j_\nu$  for free-free, with electrons assumed to interact with ions of charge  $Z_i e$  and particle density  $n_i$  is

$$j_\nu = 5.44 \times 10^{-16} \frac{g_{ff} Z_i^2 n_e n_i}{T^{1/2}} e^{-h\nu/kT} \text{ Jy sr}^{-1} \text{ cm}^{-1} \quad (1)$$

where  $g_{ff}$  is the gaunt factor for free-free. For microwave frequencies, a useful approximation is

$$g_{ff} = \frac{3^{1/2}}{\pi} \left[ \ln \frac{(2kT)^{3/2}}{\pi e^2 \nu m_e^{1/2}} - \frac{5\gamma}{2} \right] \quad \nu_p \ll \nu \ll kT/h \quad (2)$$

where  $\gamma$  is the Euler constant ( $\gamma \approx 0.577$ ) and  $\nu_p$  is the plasma frequency (Spitzer 1978, p. 58). Evaluating for  $\nu = 10^{10}$  Hz and  $T = 10^4$  K we find  $g_{ff} \approx 4.69$  and  $J(10 \text{ GHz}) = 78.8 \text{ Jy sr}^{-1}$  for  $\text{EM} = 1 \text{ pc cm}^{-6}$ . The emission measure for these clouds may be estimated from the H $\alpha$  emission shown in Figures 1 and 2. Note that  $1R = 10^6/4\pi \text{ photon cm}^{-2} \text{ s}^{-1} \text{ sr}^{-1}$  and corresponds to  $\text{EM} \approx 2 \text{ pc cm}^{-6}$  for H $\alpha$  at  $T = 10^4$  K. For LPH 201.663+1.643, the peak of the cloud is about 200R or  $\text{EM}=400$ . Using a conversion factor of  $N(H) = 8 \times 10^{21}$  for 1 mag  $E(B - V)$ , we get free-free emission of  $3.2 \times 10^4 \text{ Jy/sr}$  for  $N(H) = 2.4 \times 10^{22}$  or  $j_\nu/n_H = 1.3 \times 10^{-18} \text{ Jy sr}^{-1} \text{ atom}^{-1}$  at 10 GHz. The SFD98 map shows about 6 mag extinction ( $\tau \approx 6.5$ ) for an H $\alpha$  photon traveling completely through this cloud, so this free-free estimate should be taken as a lower limit for photons from within the cloud. If the H $\alpha$  emitting material is uniformly mixed with dust in a cloud with total optical depth  $\tau$ , the effective flux observed is

$$J_{\nu,eff} = \frac{J_\nu}{\tau} \int_0^\tau d\tau' e^{-\tau'} = \frac{J_\nu}{\tau} (1 - e^{-\tau}) \quad (3)$$

In the limit of large  $\tau$ , the flux is simply reduced by a factor of  $\tau$ . In Figure 5, the level of predicted free-free has been multiplied by a factor of 7 and appears to be in good agreement with the uniform mixture hypothesis. Of course, this result is very sensitive to the configuration of material on the front side of the cloud, so the agreement may be largely coincidental.

---

<sup>5</sup>The data are available at “<http://amundsen.swarthmore.edu/SHASSA/>”

## 5. FUTURE WORK

### 5.1. Requirements

In order to demonstrate convincingly that the excess emission detected by this work is electric dipole emission from spinning dust, the following requirements are proposed.

1. Observations for any line of sight must agree with the model over a wide frequency range (5–60 GHz) for reasonable values of the model parameters (gas and dust temperature, density, and ionization fraction). The observations must be inconsistent with free-free alone at high confidence. Simply stated, the spectral shape should exhibit a “roll-off” on both sides of the emission peak.
2. Variation in the spectrum of spinning dust emission should trace variation in the parameters as derived from spectral line information and the SFD maps. The nature of this variation should be (at least qualitatively) similar to that anticipated by the Draine & Lazarian model.
3. Alternative explanations for the excess (such as magnetic dipole emission) should be ruled out by the spectral shape. Polarimetry is also useful, as the spinning dust emission is relatively unpolarized (Lazarian & Draine 2000).

None of these requirements are met by the current paper, so our interpretation of the observed excess is only tentative. During the next few years, however, dramatically improved data will become available.

### 5.2. Prospects

There are compelling reasons to pursue this project with an interferometer in the southern hemisphere, such as CBI (Cosmic Background Imager, Padin *et al.* 2001). The synthesized beam is  $5 - 8'$ , well-matched to the  $6'$  of the IRAS (Beichman *et al.* 1988) map as reprocessed by Schlegel *et al.* (1998). CBI has 10 channels from 26 – 36 GHz, providing spectral information with high sensitivity. Many prospective targets are in the southern half of the sky, toward the Galactic center. The frequency coverage is not ideal for separation of free-free from spinning dust, but the high sensitivity ( $41\mu\text{K}$  in 900s for the highest resolution configuration) should allow clean detections and easy comparison with the Rhodes (Jonas *et al.* 1998) survey at 2.326 GHz for free-free removal. The DASI (Degree Angular Scale Interferometer, Halverson *et al.* 1998) has many of the same properties, but a larger beam of about  $20'$ , and is therefore more appropriate for comparison with the Rhodes data

(20').

The recently launched Microwave Anisotropy Probe (*MAP*; Bennett *et al.* 1997) has full-sky coverage at 22, 30, 40, 60, and 90 GHz with beams of 56, 41, 32, 21, and 14' (FWHM) respectively. These data will complement the interferometer data nicely. With data from these projects, a decisive detection of spinning dust emission may be possible in the near future.

## 6. CONCLUSIONS

We have explored a FIR-selected sample of dust clouds spanning a wide range of IR color-temperature, column density, and ionization fraction. Our target selection procedure rejected the radio-bright H II regions as poor targets, because free-free was expected to overwhelm spinning dust emission. In spite of this prejudice, one H II region (from the catalog of diffuse H II regions in Lockman, Pisano & Howard 1996; LPH) made the list, and provided a very significant detection. A dark cloud, Lynds 1622, was also detected and found inconsistent with free-free emission at a lower confidence. This is the first detection of a rising spectrum source at 8 – 10 GHz consistent with spinning dust. The amplitude of this emission per H atom apparently varies by a factor of at least 30, somewhat more than theoretically expected. Some adjustment of model parameters will be needed to explain the brightness of LPH 201.663+1.643, but the current model of Draine & Lazarian can probably accommodate the new data (Draine, 2001). Note that magnetic dipole emission from ferromagnetic or ferrimagnetic grains (Draine & Lazarian 1999) is substantially weaker than the observed signal from LPH 201.663+1.643, but significant contributions from such a mechanism cannot currently be ruled out.<sup>6</sup> Other attempts have been made to explain the large variation using 12 $\mu$ m emission as a tracer of the small grain population (de Oliveira-Costa *et al.* 2001). We caution that the interpretation of these data must remain tentative until a larger sample meeting the criteria in §5 can be obtained.

Cold neutral clouds are an obvious target choice for future work, because free-free emission is likely to be subdominant in them. Diffuse ionized gas also appears to be an excellent target, since ion-dust interactions are effective at spinning up the grains. As long as the density is low, as in the LPH list (Lockman *et al.* 1996), H II regions may be the optimal targets for future work with DASI, CBI, and *MAP*.

---

<sup>6</sup>Because this emission may be  $\sim 30\%$  polarized for aligned grains of strongly magnetic material, polarization measurements would be helpful.

This measurement is rather tenuous, as was the discovery of Galactic radio emission 60 years ago (Reber 1940). The signal was immediately interpreted as free-free (Heney & Keenan 1940) but was later recognized as synchrotron radiation. Those emission mechanisms are now essential tools for ISM research in the Milky Way and distant galaxies. With the expected increase in astronomical capability at microwave frequencies in the near future, we anticipate that spinning dust will make a useful addition to this toolbox.

We would like to thank the staff at Green Bank, especially Dana Balser, who spent 20 hours helping us with the backend software on the first day. Bruce Draine provided model emissivities and helpful discussions. Peter McCullough and John Gaustad provided  $\text{H}\alpha$  data in the regions of interest prior to publication. Shaul Hanany, Al Kogut, Alex Lazarian, Jay Lockman, and George Smoot provided helpful comments on the manuscript. Computers were partially provided by a Sun AEGP Grant. DPF is a Hubble Fellow, and was partially supported by NASA grant NAG 5-7833. DJS is partially supported by the Sloan Digital Sky Survey. This work was also supported in part by NSF grants 95-30590 and 00-97417 to CH. This research made use of the NASA Astrophysics Data System. The Green Bank 140 foot telescope was operated by the National Radio Astronomy Observatory (NRAO), which is a facility of the National Science Foundation operated under cooperative agreement by Associated Universities, Inc.

## REFERENCES

IRAS Catalogs and Atlases: Explanatory Supplement 1988, eds. Beichman, C. A., Neugebauer, G., Habing, H. J., Clegg, P. E., & Chester, T. J. (Washington, D.C.: U.S. Government Printing Office)

Bennett, C. L. *et al.* 1997, AAS, 191, #87.01

Boughn, S. P., Cheng, E. S., Cottingham, D. A., & Fixsen, D. J. 1992, ApJ, 391, L49

Cottingham, D. A. 1987, Ph.D. Thesis, Princeton Univ.

de Oliveira-Costa, A., Kogut, A., Devlin, M. J., Netterfield, C. B., Page, L. A., Wollack, E. J. 1997, ApJ, 482, L17

de Oliveira-Costa, A., Tegmark, M., Page, L., Boughn, S. 1998, ApJ, 509, L9

de Oliveira-Costa, A. *et al.* 1999, ApJ, 527, L9

de Oliveira-Costa, A. *et al.* 2001, astro-ph/0010527

Draine, B. T. 2001, priv. comm.

Draine, B. T., & Lazarian, A. 1998a, ApJ, 494, L19

Draine, B. T., & Lazarian, A. 1998b, ApJ, 508, 157

Draine, B. T., & Lazarian, A. 1999, ApJ, 512, 740

Erickson, W. C. 1957, ApJ, 126, 480

Ferrara, A., & Dettmar, R. -J. 1994, ApJ, 427, 155

Finkbeiner, D. P., Davis, M., & Schlegel, D. J. 1999, ApJ, 524, 867

Gaustad, J. E., McCullough, P. R., Rosing, W., & Van Buren, D. 2001, PASP, 113, in press (Nov. 2001)

Gawiser, E., & Silk, J. 1998, Science 280, 1405

Gregory, P. C., & Condon, J. J. 1991, ApJS, 75, 1011

Haffner, L. M., Reynolds, R. J., & Tufte, S. L. 1998, ApJ, 501, L83

Halverson, N. W., Carlstrom, J. E., Dragovan, M., Holzapfel, W. L., & Kovac, J. 1998, Proc. SPIE, 3357, 416

Henyey, L. G. & Keenan, P. C. 1940, ApJ, 91, 625

*IRAS Point Source Catalogue* 1985, Joint *IRAS* Science Working Group (Washington, DC: US Government Printing Office)

Jonas, J. L., Baart, E. E., & Nicolson, G. D. 1998, MNRAS, 297, 977

Kogut, A. *et al.* 1996, ApJ, 464, L5

Kuehr, H., Witzel, A., Pauliny-Toth, I. I. K., & Nauber, U. 1981, A&AS, 45, 367

Lazarian, A. & Draine, B. T. 2000, ApJ, 536, L15

Leitch, E. M., Readhead, A. C. S., Pearson, T. J., & Myers, S. T. 1997, ApJ, 486, L23

Lockman, F. J., Pisano, D. J., & Howard, G. J. 1996, ApJ, 472, 173 [LPH]

Lynds, B. T. 1962, ApJS, 7, 1

McCollough, P. 2001, priv. comm. [H $\alpha$  maps]

Padin, S. *et al.* 2001, ApJ, 549, L1

Purcell, E. M. 1979, ApJ, 231, 404

Reber, G. 1940, ApJ, 91, 621

Salter, Chris 2001 priv. comm.

Schlegel, D. J., Finkbeiner, D. P., & Davis M. 1998, ApJ, 500, 525 [SFD]

Spitzer, L. 1978, *Physical Processes in the Interstellar Medium*, Wiley, New York

Vrba F.J., Strom S.E., & Strom K.M. 1976, AJ, 81, 958

Wright, A. E., *et al.* 1991, MNRAS, 251, 330

Table 1. Target list

Name	$\alpha_{2000}$	$\delta_{2000}$	result	comment
L1622	05 54 23	+01 46 54	detected	dark cld
LPH 201.663+1.643	06 36 40	+10 46 28	detected	diffuse H II
L1591	06 09 55	+13 44 34	ND	dark cld
IRAS 07225–1617	07 24 47	–16 23 21	weak	IRAS source
IRAS 15522–2540	15 55 16	–25 49 40	no 10	IRAS source
VSS II-79	16 33 58	–23 43 48	neg corr	near L1709C
IRAS 18146–1200	18 17 29	–11 58 52	8 only	near H II
IRAS 19441+2926	19 46 08	+29 33 34	ND	IRAS source
IRAS 23339+4811	23 36 23	+48 28 01	ND	IRAS source
IRAS 23350+4815	23 37 28	+48 32 18	ND	IRAS source

Note. — List of targets observed. ND = not detected. Most of these have other names in the literature. VSS II-79 has a significant negative correlation with dust emission, perhaps from an H II shell around the dust filament. LPH = Lockman, Pisano, & Howard (1996), IRAS = IRAS Science Working Group (1985), L = Lynds (1962), and VSS = Vrba, Strom, & Strom (1976).

Table 2. Correlation slopes

Name	$\nu$	For RCP	Ret RCP	For LCP	Ret LCP	Avg	nsig
L1622	5.00	$1.29 \pm 0.39$	$3.49 \pm 0.84$	$0.48 \pm 0.38$	$3.05 \pm 0.77$	$1.31 \pm 0.25$	5.3
L1622	8.25	$1.25 \pm 0.29$	$0.26 \pm 0.37$	$0.67 \pm 0.41$	$0.52 \pm 0.35$	$0.75 \pm 0.17$	4.4
L1622	8.25	$1.14 \pm 0.37$	$1.24 \pm 0.44$	$1.05 \pm 0.38$	$1.11 \pm 0.33$	$1.13 \pm 0.19$	6.1
L1622	9.75	$1.65 \pm 0.67$	$0.76 \pm 0.77$	$0.84 \pm 0.73$	$0.78 \pm 0.65$	$1.03 \pm 0.35$	2.9
LPH	5.00	$53.16 \pm 5.28$	$57.01 \pm 5.68$	$54.12 \pm 5.39$	$58.05 \pm 5.90$	$55.41 \pm 2.77$	20.0
LPH	8.25	$25.45 \pm 1.69$	$25.92 \pm 1.91$	$29.16 \pm 1.93$	$29.50 \pm 2.25$	$27.22 \pm 0.96$	28.4
LPH	9.75	$23.96 \pm 2.09$	$23.33 \pm 1.70$	$27.89 \pm 2.49$	$27.17 \pm 1.90$	$25.25 \pm 0.99$	25.4

Note. — Correlation slopes for Forward and Return scans, RCP and LCP polarizations. These correlation slopes are for  $T_B$  vs. a prediction of  $50\mu\text{K}/I_{100}$  where  $I_{100}$  is the DIRBE-temperature-corrected IRAS intensity at 100 $\mu\text{m}$  in MJy/sr. This temperature-corrected map may be obtained by dividing the SFD98  $E(B - V)$  prediction by 0.0184. The prediction used includes a factor of 1/2 for single polarization measurements, so RCP and LCP are combined by averaging, not adding. Values in the table may be multiplied by 50 to obtain units of  $\mu\text{K}/I_{100}$  in order to compare to e.g. de Oliveira-Costa *et al.* (1999). Note that Lynds 1622 was observed twice at 8.25 GHz.

Table 3. Emissivity per H

Name	$N(H)$	$j_\nu(5 \text{ GHz})/n_{\text{H}}$	8.25 GHz	9.75 GHz
	$\times 10^{21} \text{ cm}^{-2}$	$\text{Jy sr}^{-1} \text{ H}^{-1}$	$\text{Jy sr}^{-1} \text{ H}^{-1}$	$\text{Jy sr}^{-1} \text{ H}^{-1}$
L1622	18	$7.8 \pm 3.9 \times 10^{-19}$	$6.6 \pm 1.3 \times 10^{-19}$	$10.1 \pm 3.4 \times 10^{-19}$
LPH	27	$147 \pm 17 \times 10^{-19}$	$191 \pm 7 \times 10^{-19}$	$247 \pm 10 \times 10^{-19}$

Note. — Emissivity.  $N(H)$  is estimated by using the SFD98  $E(B - V)$  extinction estimate and a conversion factor of  $N(H) = 8 \times 10^{21} \text{ cm}^{-2}$  per magnitude.

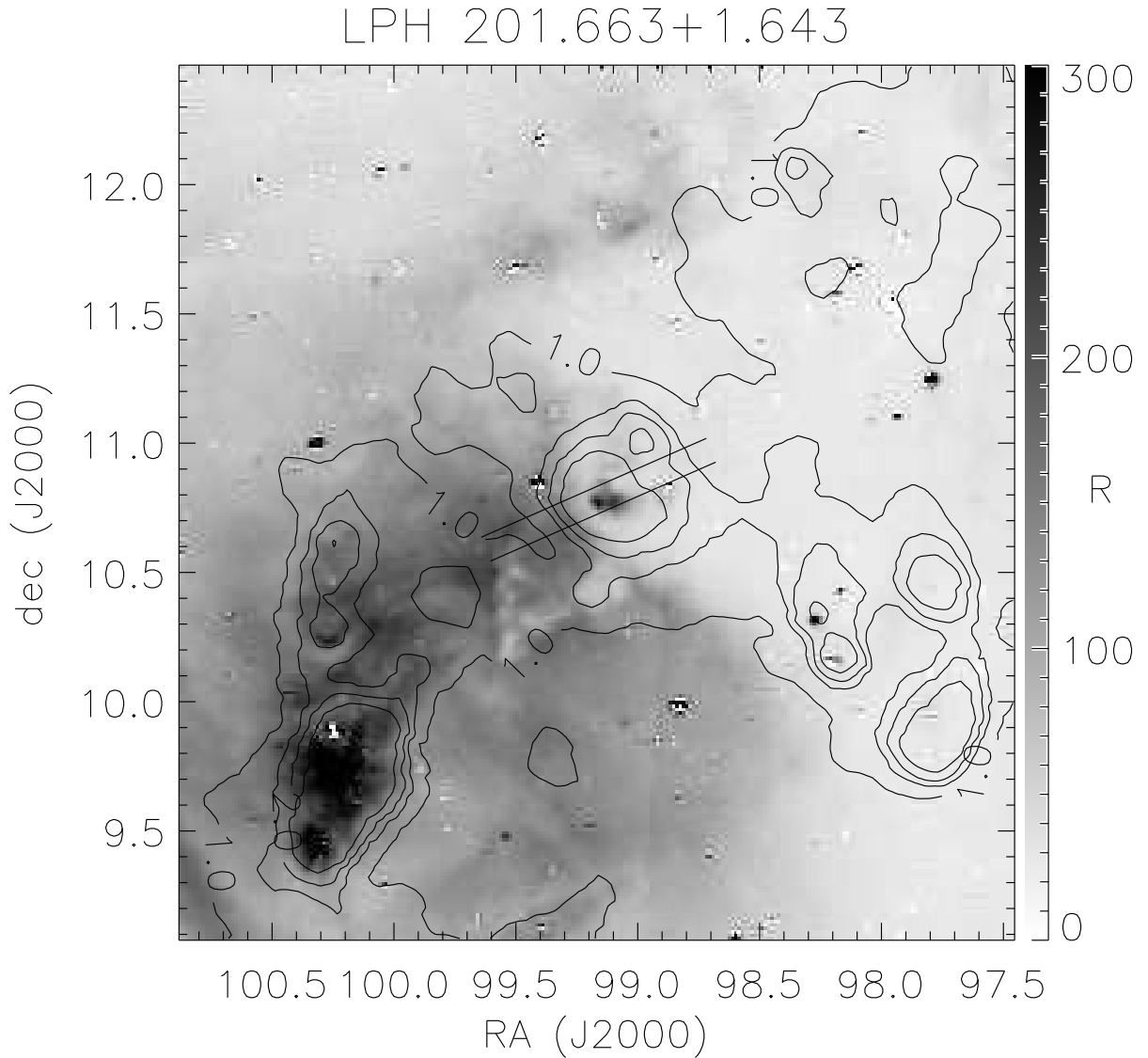


Fig. 1.— Scan location for the LPH cloud (*black lines*), overplotted on SHASSA (Gaustad *et al.* 2001) H $\alpha$  (*grayscale*) and SFD98  $E(B - V)$  (*contours*). Contour levels are 1,1.5,2,3 mag. H $\alpha$  brightness is measured in Rayleighs with the scale on the right. One Rayleigh is  $10^6/4\pi$  photon cm $^{-2}$ s $^{-1}$ sr $^{-1}$ .

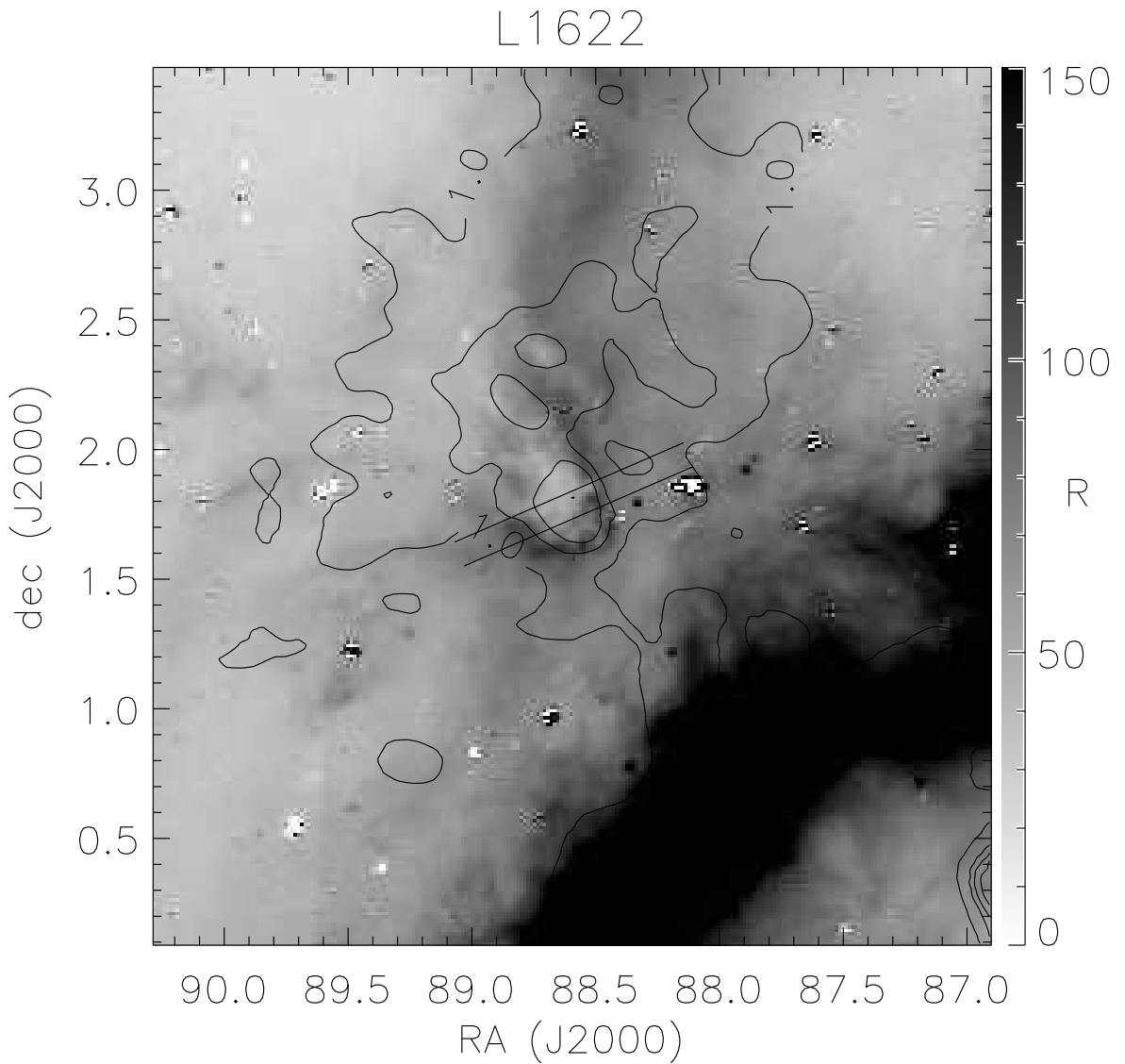


Fig. 2.— Scan location for Lynds 1622 (*black lines*), overplotted on H $\alpha$  (*grayscale*) and SFD98  $E(B - V)$  [mag] (*contours*).

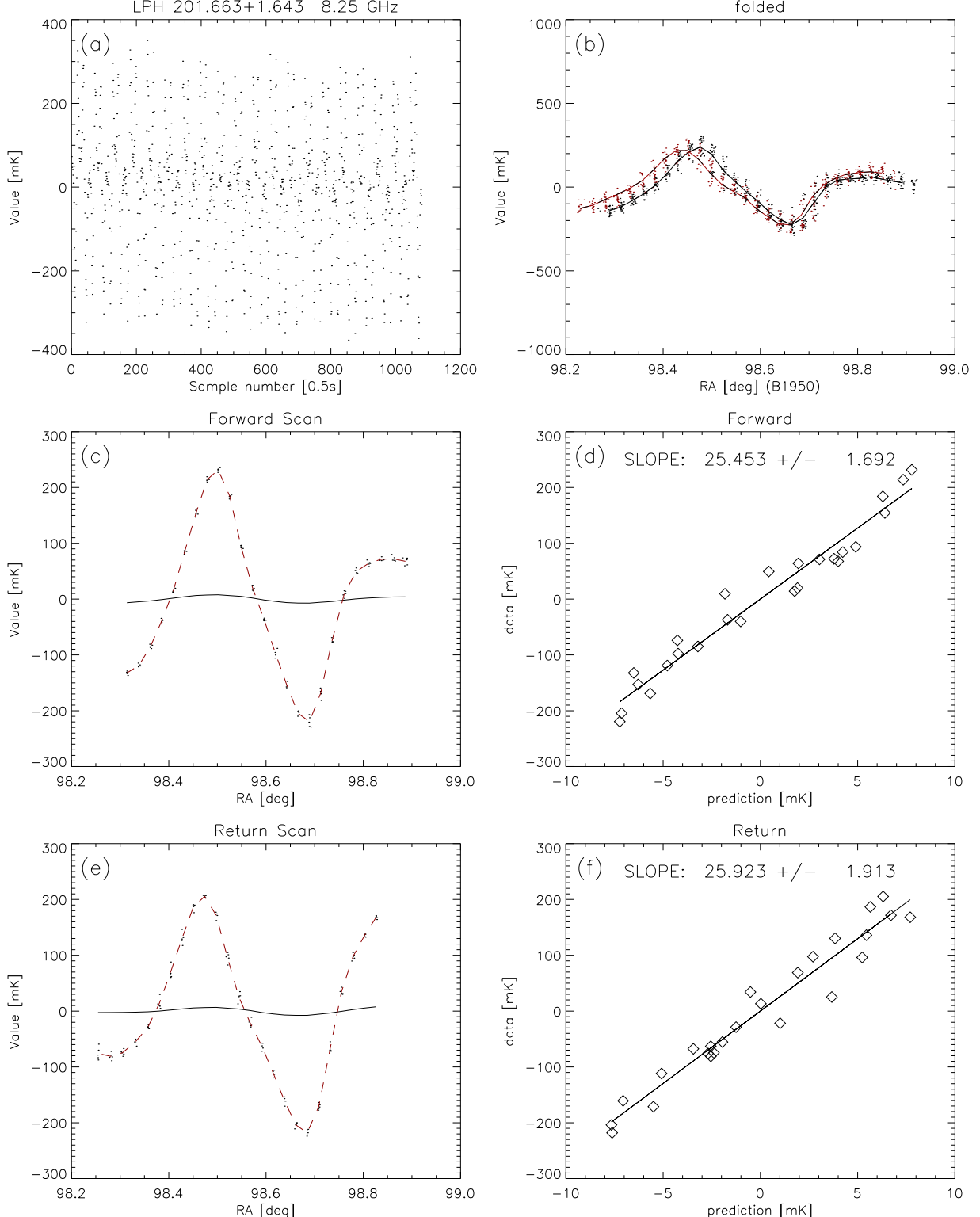


Fig. 3.— For the diffuse H II region LPH 201.663+1.643: (a) observed differences vs. time; (b) differences folded vs. RA for (black) forward and (red) return scans; (c) (dashed) data and (solid) SFD-based prediction using conversion factor for 10 GHz from de Oliveira-Costa *et al.* (1999) for the forward scan; (d) correlation of data vs. prediction for the forward scan; (e) same as (c) for the return scan; and (f) same as (d) for the return scan. Correlation does not hold exactly at 10 GHz for the prediction, and the conversion factor at 8 GHz

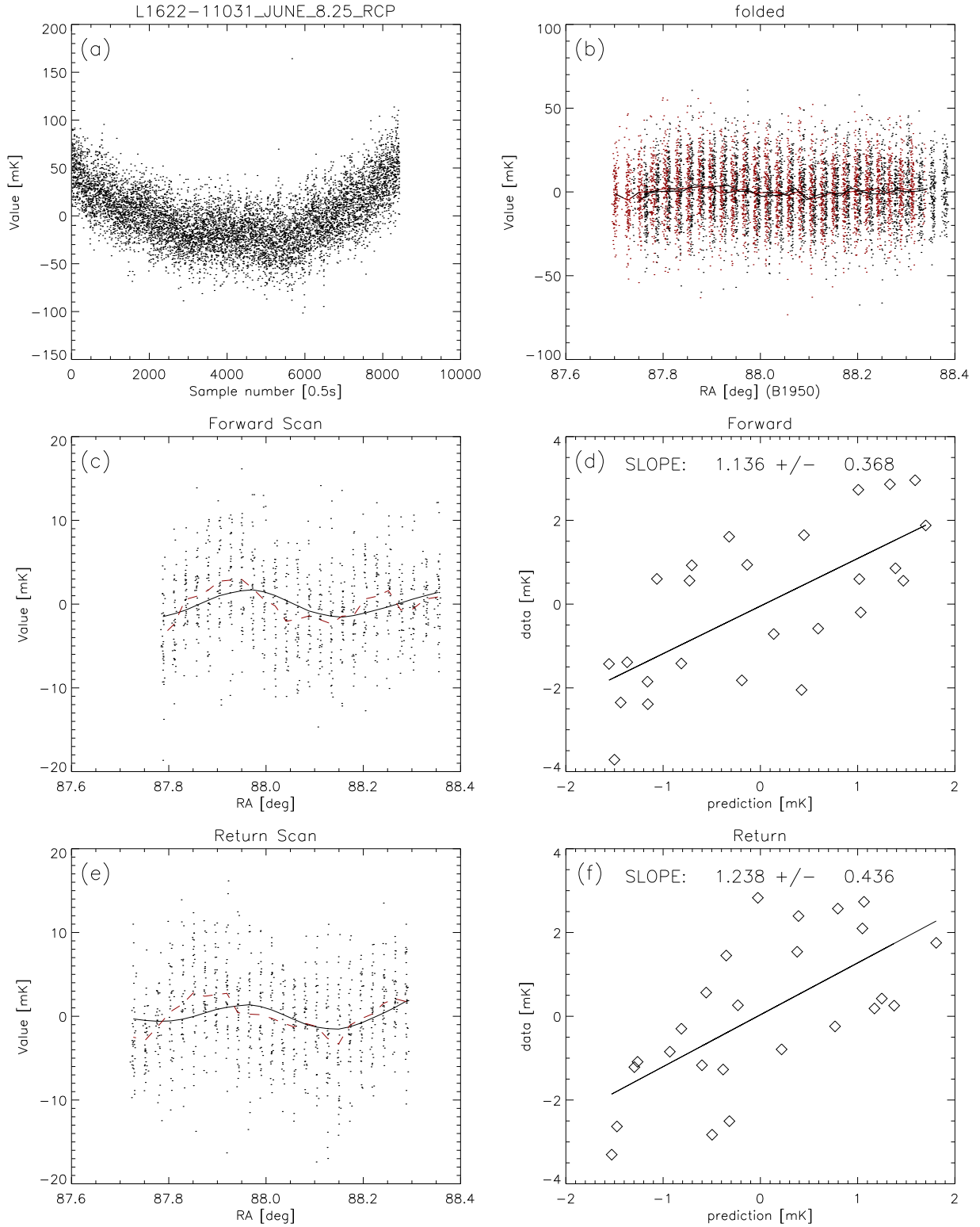


Fig. 4.— Same as Figure 3 but for Lynds 1622. Notice that the correlation slope is substantially less than unity in this region.

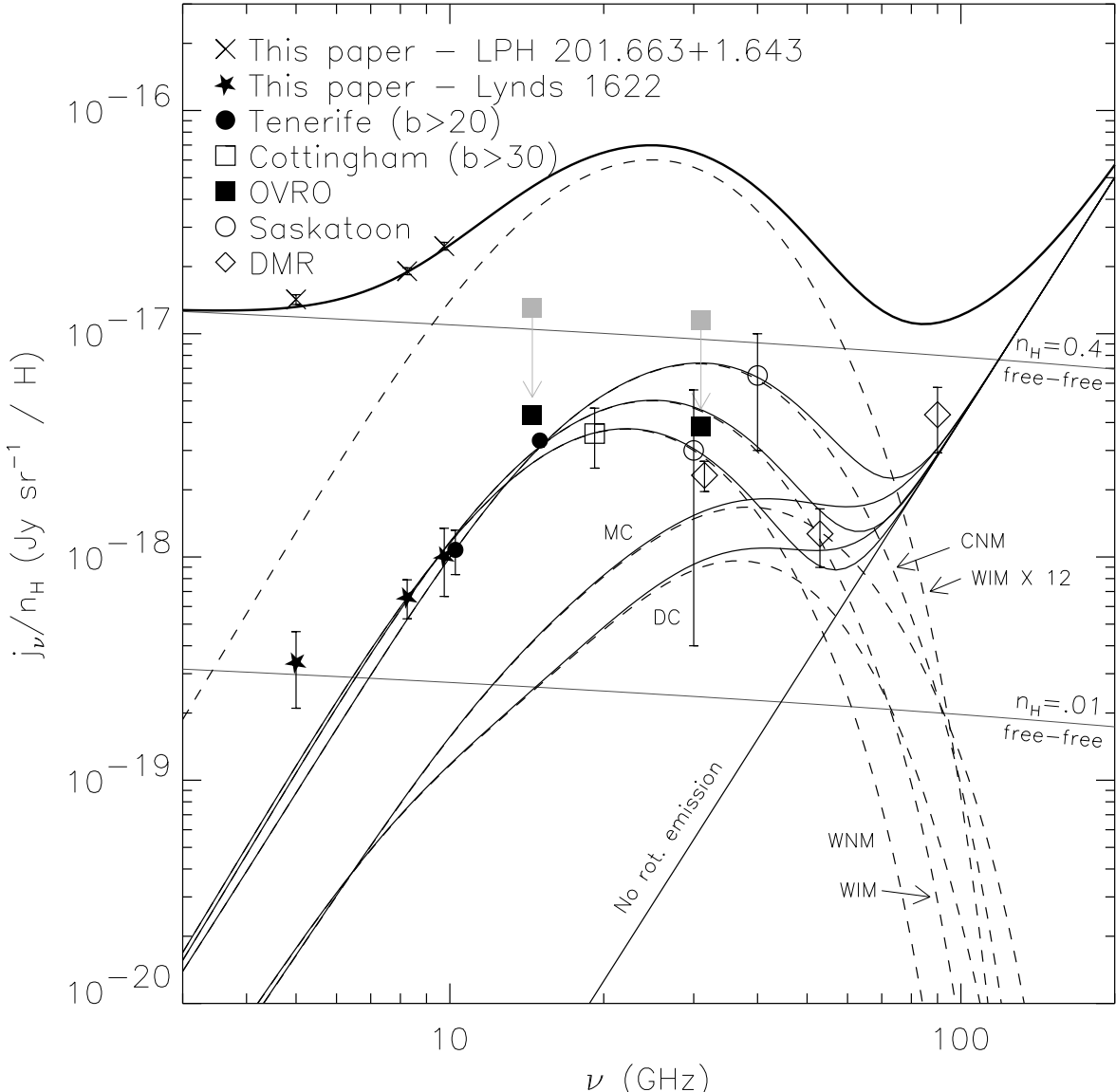


Fig. 5.— Model Dust emissivity per H atom for DC, MC, CNM, WNM, and WIM conditions (as in Draine & Lazarian 1998b, Figure 9). Solid thin lines are total emissivity; dashed lines are rotational emission. Gray lines are emission from free-free for given  $n_H$ , or rather  $\langle n_e n_p \rangle / \langle n_H \rangle$  averaged along the line of sight. The top thick line is the sum of free-free, vibrational dust, and 10 times the WIM spinning dust model, shown for reference. Also shown are measurements from the *COBE*/DMR (*open diamonds*) from Finkbeiner *et al.* (1999), similar to Kogut *et al.* (1996); Saskatoon (*open circles*) (de Oliveira-Costa *et al.* 1997); the Cottingham & Boughn 19.2 GHz survey (*open square*) (de Oliveira-Costa *et al.* 1998), OVRO data (*solid squares*) (Leitch *et al.* 1997); Tenerife data (*solid circles*) (de Oliveira-Costa *et al.* 1999); and this paper: LPH 201.663+1.643 (*crosses*) and L1622 (*stars*). The OVRO points have been lowered a factor of 3 relative to Draine & Lazarian (1998b, Figure 9), because the unusual dust temperature near the NCP caused an underestimate of the H column density along those lines of sight. Given the large range of model curves,